Thermo-responsive Amphiphilic Di- and Triblock Copolymers Based on Poly(N-isopropylacrylamide) and Poly(methoxy diethylene glycol acrylate): Aggregation and Hydrogel Formation in Bulk Solution and in Thin Films

André Laschewsky, Peter Müller-Buschbaum, and Christine M. Papadakis

Abstract

In this feature, we provide a comprehensive view and conclusions on recent investigations on the micellar aggregation of amphiphilic model polymers, the subsequent hydrogel formation, and the thermoresponsive behavior. The results obtained in bulk solution as well as in thin films are combined and compared, from the structural as well as kinetic point of view. The studies used two extensive series of diblock and symmetrical triblock copolymers, which were prepared by reversible addition-fragmentation chain transfer (RAFT). Derived from the thermo-responsive parent polymers poly(N-isopropylacrylamide) (PNIPAM) and poly(methoxy diethylene glycol acrylate) (PMDEGA), respectively, both series exhibit a lower critical solution type phase transition in aqueous media in the range of 30–40 °C. The model polymers consist of a long hydrophilic, thermo-responsive middle block, which is end-capped by two relatively small, but strongly hydrophobic blocks made from various vinyl polymers, preferentially from polystyrene. Their aggregation and hydrogel formation as well as their thermo-responsive behavior are systematically studied in dilute and concentrated aqueous solution as well as in thin films. For that, complementary methods were applied such as turbidimetry, fluorescence correlation spectroscopy (FCS), dynamic light scattering (DLS), small-angle X-ray (SAXS) and neutron scattering (SANS), rheology, white light interferometry, atomic force microscopy (AFM), optical probes, X-ray (XRR) and neutron reflectivity (XRR), grazing-incidence small-angle X-ray (GISAXS) and neutron scattering (GISANS) as well as attenuated total reflectance Fourier transform infrared spectroscopy (ATR-FTIR). All amphiphilic block copolymers self-organize at several hierarchical levels in bulk solution as well as in thin films. First, the association of the hydrophobic building blocks results in micelle-like aggregates. Then, the micelles cluster and eventually form networks, that make the systems gel. At elevated temperatures, the hydrophilic blocks undergo a collapse transition, inducing major structural changes at the molecular as well as supramolecular levels. Characteristic differences between PNIPAM and PMDEGA based solutions and thin films are worked out, concerning the self-organization, the width and hysteresis of the transition and the switching kinetics. Thin films of PNIPAM and PMDEGA based polymers differ with respect to long ranged correlations and the stability against dewetting. When probing polymer collapse, aggregation behavior, segmental dynamics and mechanical properties of the micellar solutions and the hydrogels,

A. Laschewsky (✉)
Department of Chemistry, Universität Potsdam, Karl-Liebknecht-Str. 24-25, Potsdam-Golm, D-14476 Germany
e-mail: Laschews@uni-potsdam.de

P. Müller-Buschbaum (✉) • C.M. Papadakis (✉)
Physik-Department, Technische Universität München, Lehrstuhl für Funktionelle Materialien/Fachgebiet Physik Weicher Materie, James-Franck-Str.1, Garching D-85748, Germany
e-mail: muellerb@ph.tum.de; papadakis@tum.de

G. Sadowski and W. Richtering (eds.), *Intelligent Hydrogels*, Progress in Colloid and Polymer Science 140,
DOI 10.1007/978-3-319-01683-2__2,

both the chain architecture and the chemical nature of the thermo-responsive block are found to play an important role for the detailed phase behavior.

Keywords
Triblock copolymer • Amphiphile • Polymer micelle • Hydrogel • Lower critical solution temperature • Aggregation behavior • Phase transition kinetics • Thin film

Introduction

Polymer hydrogels can be produced by a number of strategies. Common to all is the need of cross-links that keep the polymer network together, either by chemical or by physical bonds [1, 2]. The latter strategy has the advantage to be reversible, and thus to enable the reshaping and the assembly (or disassembly) of hydrogels by adapting physical parameters. A class of polymers particularly suited to form hydrogels, are amphiphilic block copolymers, which aggregate into micelle-like structures at low concentration, and eventually gel due to the formation of permanent or temporary networks at high concentrations [3–5] Characteristically, the hydrophobic blocks in such copolymers are responsible for the primary aggregation, while the hydrophilic blocks ensure the compatibility of the aggregates with the aqueous matrix and control the extent of swelling of the gels [4–7]. For long, hydrogel formation of simple AB diblock copolymers consisting of a hydrophilic block "A" and a hydrophobic block "B" has been studied. In recent years, the interest has been extended to the more complex symmetrical triblock copolymers of the BAB type, i.e., to copolymers which are made of a hydrophilic center and two hydrophobic ends [8–10]. In fact, for amphiphilic triblock copolymers, the self-assembly depends not only on the chemical nature of the A and B blocks, and on their absolute as well as their relative lengths, but also on the block sequence (ABA or BAB). While ABA systems tend to form core-shell micelles in aqueous solution similar to diblock copolymers [6], copolymers of the BAB type may associate into flower-like micelles in dilute solution, with both hydrophobic blocks of the same macromolecule being part of the same micellar core [10, 11]. The flower-like micelles may eventually evolve to clusters of interconnected micelles and finally to a network, when the polymers share their hydrophobic end blocks between two micelles with increasing concentration. Such bridging conformations will favor gelation of the systems, as they provide additional physical cross-links [5, 10–12]. From this point of view, the molecular structure of amphiphilic BAB polymers reflects the one of hydrophobically end-capped associative polymers, which is known as efficient associative thickeners [13–16].

The possibilities for block copolymer based hydrogels – and inevitably also their complexity – has been increased by superposing the concept of so-called "smart" systems onto their supramolecular self-assembly. In these smart hydrogels, the swelling/deswelling behavior of the polymers (in our specific case in water) is controlled by an external stimulus, such as a specific value of pH or temperature [17–21]. In this context, the use of amphiphilic triblock copolymers that exhibit a lower critical solution temperature (LCST) for switching hydrogels, has found particular interest in recent years [22–25]. LCST behavior in aqueous media is widespread amidst polar non-ionic polymers [26–28], and the switching process is non-invasive, i.e., can be achieved in a materially closed system. Classical examples for thermo-responsive polymers exhibiting a LCST in water under ambient pressure are poly(ethylene oxide) (also often named poly(ethylene glycol), PEG), poly(vinyl alcohol), methylcellulose, elastin-like proteins, and poly(N-isopropyl acrylamide), which is arguably the best studied representative of the class [29–31]. Thermo-responsive triblock copolymers derived from PNIPAM with, for instance, polystyrene (**PS**) end blocks in aqueous solution have been shown to form flower-like core-shell micelles with a thermoresponsive shell [32, 33], and at high polymer concentration, all the classical block copolymer mesophases [32, 34].

The synthesis of amphiphilic thermo-responsive block copolymers had been hampered for long by synthetic difficulties. In fact, the highly polar and often hygroscopic thermo-responsive blocks tolerate only in exceptional cases the rather harsh classical methods to prepare block copolymers, such as living ionic polymerization [35]. The situation has much changed with the advent of the reversible deactivation radical polymerization (RDRP) methods (formerly often called "controlled free radical polymerization") [36], which emerged in the late 1990s. Since then, the synthetic toolkit for making amphiphilic (including thermo-responsive) block copolymers has been dramatically enlarged and has increasingly enabled the possibilities to tailor specific polymer designs [37, 38]. In particular, we have profited from these advancements for preparing two series of block copolymers via the radical addition-fragmentation chain transfer (RAFT) polymerization method [39, 40]. The series are based on the use of the well-established poly(N-isopropyl

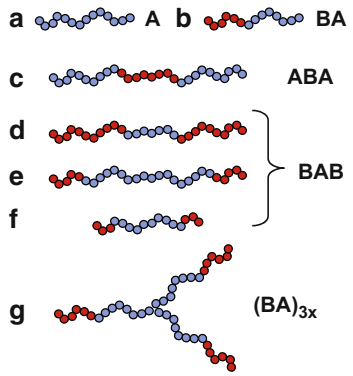

Scheme 1 Schematic architectures of the thermo-responsive polymers studied: (**a**) homopolymer references, (**b**) amphiphilic BA diblock copolymer, (**c**) amphiphilic ABA symmetrical triblock copolymer, (**d**–**f**) amphiphilic BAB symmetrical triblock copolymers of varying relative and absolute block sizes, (**g**) amphiphilic $(BA)_{3x}$ 3-arm star block copolymer (*light blue/light grey* shade = thermo-responsive block A, *red/dark grey* shade = hydrophobic block B)

acrylamide) PNIPAM [29], and of the – so far – little studied poly(methoxy diethylene glycol acrylate) PMDEGA [41] as hydrophilic and thermo-responsive building blocks. Both PNIPAM and PMDEGA exhibit a LCST in the physiologically particularly interesting range of 30–40 °C. Yet, as will be shown below, both polymers show characteristic differences with respect to their thermo-responsive behavior despite their very close LCST values and thus ought to be considered as complementary rather than competitive options for implementing "intelligent" hydrogel systems.

Structural Features of the Investigated Model Polymers

In order to gain more insight in the temperature-dependent self-organization of such amphiphilic thermo-responsive block copolymers, we varied the macromolecular structure of our model systems broadly (Scheme 1), by varying the molecular architecture (BA diblock *versus* BAB symmetrical triblock *versus* $(BA)_{3x}$ 3-arm star block copolymers), as well as the relative and absolute sizes of the thermo-responsive hydrophilic A and the permanently hydrophobic B blocks [24, 25, 42–48]. For comparison, these systematic variations were complemented by PNIPAM and PMDEGA homopolymer references and by some ABA symmetrical triblock copolymers, in which the permanently hydrophobic block forms the central block that is framed by the thermo-responsive hydrophilic blocks.

For the various amphiphilic block copolymers, we end-capped the thermo-responsive blocks by – mostly short – hydrophobic blocks, with a particular emphasis on **PS** as model hydrophobic polymer (see Tables 1 and 2). In order to get more insight into the structure–property relationships of such smart block copolymers, we varied systematically their most important macromolecular structural variables, namely, the absolute and relative block lengths, and the polymer architecture. Thus, we prepared amphiphilic AB diblock, BAB triblock, and $(BA)_{3x}$ triarm diblock star polymer analogs. Moreover, we have explored the role of the nature of the hydrophobic blocks, by varying the hydrophobicity of the repeat units as well as their glass transition temperatures [24], to learn about the effect of glassy or "molten" hydrophobic micellar cores. Last but not least, we have incorporated deuterated hydrophobic blocks into the polymers, too [44–48]. This facilitates the use of neutron scattering [49, 50] and spectroscopy techniques [51, 52], which are powerful tools for structural as well as dynamic investigations of mesoscopic systems.

From the pool of RDRP methods, we selected the RAFT method for synthesizing the polymers. First of all, RAFT is particularly suited to polymerize acrylic and styrenic monomers, which have been in our primary focus. Furthermore, the RAFT method confers two non-identical end groups to the polymers, which allow in a rather unique way to verify the quality of polymer intermediates and to support the – generally cumbersome – molecular characterization of amphiphilic copolymers by end-group analysis [43, 53, 54]. Detailed molecular information on the polymers studied is a keystone to interpret the results of the various investigations correctly, to maximize the reliable information that can be extracted, and to deduce general insights into such thermo-responsive supramolecular systems. Tables 1 and 2 summarize the two series of amphiphilic block copolymers synthesized, based on the thermo-responsive blocks PNIPAM and PMDEGA, respectively. The corresponding representative chemical formulas are illustrated in Figs. 1 and 2.

The variation of the hydrophobic B blocks in the copolymers of **PNIPAM** allowed us to elucidate the effects of the hydrophobicity of the various repeat units (growing with **PS** < **PtbS** and **PDBBA** < **PEHA** < **PODA**) as well as of their glass transition temperatures (growing with **PEHA** < **PDBBA** < **PODA** < **PS** < **PtbS**) on the aggregation behavior and thermo-sensitivity [24].

General Thermosensitivity of the Polymers in Aqueous Solution

While the PNIPAM and PMDEGA homopolymers dissolved easily in water at 20 °C, the dissolution/dispersion of the block copolymers required special measures, such as extended times for dissolution under shaking and/or the dispersion in non-selective organic solvents before mixing with water and removal of the cosolvent by

Table 1 Composition of the PNIPAM-containing homopolymers and amphiphilic block copolymers, and their cloud points in dilute aqueous solution

Entry	Polymer	M_n [10^3 Da]	DP_n of hydrophobic blocks	DP_n of PNIPAM block	Cloud point[a] [°C]	Ref.
	Homopolymers					
1	**$PNIPAM_{320}$**	36	–	320	31.0	[43]
2	**nbc-$PNIPAM_{340}$**[b]	39	–	340	30.0[c]	[55, 56]
3	**$PNIPAM_{430}$**	49	–	430	31.0	[43]
4	**$PNIPAM_{580}$**	66	–	580	31.0	[24]
	Diblock copolymers BA					
5	**P(S_{50}-$NIPAM_{160}$)**	23	50	160	31.6	[42, 46]
	Triblock copolymers ABA					
6	**P($NIPAM_{80}$-S_{27}-$NIPAM_{80}$)**	21	27	160	30.5	[43]
7	**P($NIPAM_{105}$-S_{30}-$NIPAM_{105}$)**	27	30	210	30.0	[43]
	Triblock copolymers BAB					
8	**P(tbS_9-$NIPAM_{280}$-tbS_9)**	34	17	280	31.5	[24]
9	**P(tbS_{17}-$NIPAM_{490}$-tbS_{17})**	60	34	490	31.5	[24]
10	**P(S_{11}-$NIPAM_{185}$-S_{11})**	23	22	185	31.0	[43]
11	**P(S_{11}-$NIPAM_{280}$-S_{11})**	34	22	280	31.2	[44]
12	**P(S_{11}-$NIPAM_{370}$-S_{11})**	44	22	370	31.3	[44]
13	**P(S_{15}-$NIPAM_{185}$-S_{15})**	24	30	185	31.0	[43]
14	**P(S_{24}-$NIPAM_{550}$-S_{24})**	67	48	550	31.5	[24]
15	**P(S_{30}-$NIPAM_{530}$-S_{30})**	66	61	530	31.5	[24]
16	**P(S_{40}-$NIPAM_{790}$-S_{40})**	98	81	790	31.5	[24]
17	**P(S_{45}-$NIPAM_{650}$-S_{45})**	82	89	650	31.5	[24]
18	**P(S_{60}-$NIPAM_{700}$-S_{60})**	92	119	700	31.5	[24]
19	**P($d8S_{11}$-$NIPAM_{220}$-$d8S_{11}$)**	27	22	220	31.2	[47, 48]
20	**P($d8S_{10}$-$NIPAM_{390}$-$d8S_{10}$)**	27	46	390	31.5	[44, 45]
21	**P($DBBA_8$-$NIPAM_{310}$-$DBBA_8$)**	40	16	310	31.5	[24]
22	**P(EHA_{11}-$NIPAM_{380}$-EHA_{11})**	47	21	380	31.5	[24]
23	**P(EHA_{18}-$NIPAM_{610}$-EHA_{18})**	77	35	610	31.5	[24]
24	**P(EHA_{25}-$NIPAM_{700}$-EHA_{25})**	88	50	700	31.5	[24]
25	**P(EHA_{30}-$NIPAM_{670}$-EHA_{30})**	87	60	670	31.5	[24]
26	**P(ODA_6-$NIPAM_{280}$-ODA_6)**	35	11	280	31.5	[24]
27	**P(ODA_{18}-$NIPAM_{800}$-ODA_{18})**	100	36	800	31.5	[24]
28	**P(ODA_{27}-$NIPAM_{1050}$-ODA_{27})**	140	54	1050	31.5	[24]

[a] At 1 g L^{-1} (heating run, onset of turbidity)
[b] Bearing two short hydrophobic butylsulfanylthiocarbonylsulfanyl end groups
[c] At 0.25 g L^{-1} via dynamic light scattering

evaporation or dialysis, in particular when bearing relatively long hydrophobic blocks (number average degree of polymerization $DP_n \geq 15$). Only copolymers with very short hydrophobic blocks ($DP_n < 12$) dissolved rather readily in water.

Turbidimetry of dilute aqueous solutions was used to map the general trends of thermo-responsive behavior of the various polymer structures. Already at this level, a major difference between the PNIPAM-based and the PMDEGA-based polymers becomes evident. For the PNIPAM-based polymers, a nearly constant cloud point of 30–32 °C is observed, independent of the molar mass of the polymers, the nature of the end groups (defined by the specific RAFT agent used), length and nature of the hydrophobic blocks, or the type of copolymer architecture (homopolymer, BA diblock as well as BAB and ABA triblock copolymers), as illustrated in Fig. 3 [24]. Also, variation of the polymer concentration between 0.2 and 40 wt% only marginally affected the position of the cloud points (see also Fig. 6 below) [24]. This is in good agreement with the literature, in particular also with reports on the missing effect of hydrophobic end groups or attached blocks, respectively, if the PNIPAM block outpasses a minimum molar mass ($> 10^4$), and if the hydrophobic end groups are equivalent to a hexadecyl chain or bigger [62, 63]. This effect has been attributed to local micro-phase separation in the aqueous environment, and to the resulting

Table 2 Composition of the PMDEGA-containing homopolymers and amphiphilic block copolymers studied and their cloud points in dilute aqueous solution

Entry	Polymer	M_n [10^3 Da]	DP_n of hydrophobic blocks	DP_n of PMDEGA block	Cloud point[a] [°C]	Ref.
	Homopolymers					
29	**$PMDEGA_{53}$**[b]	10	–	53	24.5	[41]
30	**$PMDEGA_{138}$**[c]	17	–	100	45[d]	[57, 58]
31	**$PMDEGA_{153}$**[b]	27	–	153	38.3	[41]
32	**$PMDEGA_{513}$**[b]	90	–	513	41.2	[41]
	Diblock copolymers BA					
33	**$P(S_{11}\text{-}MDEGA_{101})$**[e]	19	11	101	34.6	[41]
34	**$P(S_{11}\text{-}MDEGA_{172})$**[e]	31	11	172	38.0	[41]
35	**$P(S_{11}\text{-}MDEGA_{275})$**[e]	49	11	275	38.9	[41]
36	**$P(S_{11}\text{-}MDEGA_{331})$**[e]	59	11	331	40.0	[41]
37	**$P(S_{11}\text{-}MDEGA_{513})$**[e]	91	11	513	40.1	[41]
	Triblock copolymers BAB					
38	**$P(S_8\text{-}MDEGA_{41}\text{-}S_8)$**[b]	10	16	41	20.5	[25]
39	**$P(S_8\text{-}MDEGA_{53}\text{-}S_8)$**[b]	12	16	53	22.1	[25]
40	**$P(S_8\text{–}MDEGA_{93}\text{-}S_8)$**[b]	19	16	93	26.0	[25]
41	**$P(S_8\text{-}MDEGA_{180}\text{-}S_8)$**[b]	34	16	180	30.1	[25]
42	**$P(S_8\text{-}MDEGA_{337}\text{-}S_8)$**[b]	61	16	337	33.8	[25]
43	**$P(S_8\text{-}MDEGA_{452}\text{-}S_8)$**[b]	81	16	452	35.4	[25]
44	**$P(S_8\text{-}MDEGA_{659}\text{-}S_8)$**[b]	117	16	659	38.1	[25]
45	**$P(S_{11}\text{-}MDEGA_{126}\text{-}S_{11})$**[f]	24	22	125	36.6[d]	[58–60]
46	**$P(S_{15}\text{-}MDEGA_{550}\text{-}S_{15})$**[b]	99	30	550	37	[61]
	3-arm star block copolymers					
47	**$P(MDEGA_{78}\text{-}S_8)_3$**[g]	45	23	234	27.2	[41]
48	**$P(MDEGA_{231}\text{-}S_8)_3$**[g]	124	23	693	34.1	[41]

[a]Cloud points at 3.0 g L^{-1} (heating run, onset of turbidity)
[b]Using RAFT agent 1,2-bis[4-(*tert*-butoxycarbonyl)benzyl sulfanylthiocarbonylsulfanyl] ethane
[c]Using RAFT agent 1-[(4-methoxybenzyl)sulfanylthiocarbonylsulfanyl] propane
[d]Cloud points at 1.0 g L^{-1} (heating run, onset of turbidity)
[e]Using RAFT agent 1-[(4-carboxybenzyl)sulfanylthiocarbonylsulfanyl] butane
[f]Using RAFT agent dibenzyltrithiocarbonate
[g]Using RAFT agent 1,1,1-tris-[3-(4-(*tert*-butoxycarbonyl) benzylsulfanylthiocarbonyl sulfanyl) propanoyloxy] ethane

efficient shielding of the associated hydrophobic components from contact with water [63, 64].

In striking contrast, PMDEGA-based polymers show a very pronounced effect of the molar mass even up to high molar masses (Fig. 3). Moreover, the effect of the molar mass is counter-intuitive, as even for hydrophilic end groups, the cloud point apparently increases with increasing molar mass [41]. Furthermore, the cloud points are very sensitive to the chemical nature of low or high molar mass end groups (and thus to the specific RAFT agent used and to the length of the hydrophobic block(s) attached), as well as to the polymer architecture. Diblock, triblock and star block copolymers even of identical ratio of hydrophilic-to-hydrophobic block sizes exhibit significantly varying phase transition temperatures (Table 2, Fig. 3). In parallel, the cloud point of dilute as well as concentrated aqueous solutions of PMDEGA-based polymers display a marked dependence on the polymer concentration (Fig. 4) [25, 41]. With increasing concentration, the cloud point passes through a minimum, which shifts to lower concentrations with increasing molar mass, in agreement with predictions from simple thermodynamics.

Another striking difference is the different kinetics of the collapse or reswelling processes of the two different thermo-responsive blocks. Turbidimetry studies of the PMDEGA-based polymers show virtually no difference between the heating and cooling curves when slow rates were applied (as 0.1 °C/min), i.e., the collapse and reswelling of the polymer coils do not show a notable thermal hysteresis [41]. In contrast, PNIPAM-based polymers exhibit characteristic differences between the heating and cooling curves in turbidimetry [24, 42, 44]. The notable hysteresis is putatively attributed to a reorganization process of the PNIPAM coils above the cloud point, where part of the secondary amide moieties form hydrogen bonds between neighboring repeat units instead of with water as below the phase transition [65].

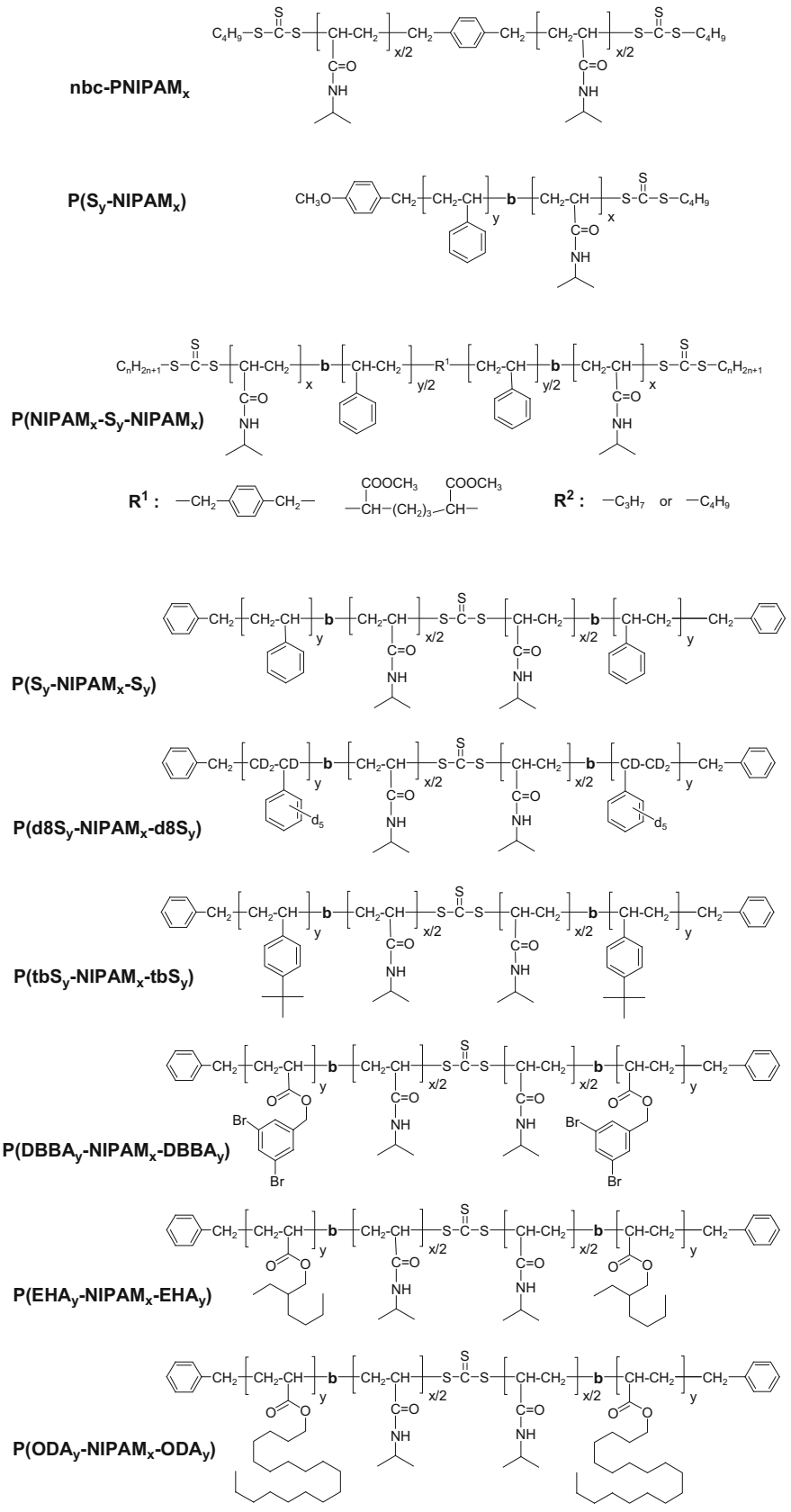

Fig. 1 General chemical structures of the synthesized polymers based on poly(N-isopropyl acrylamide) PNIPAM

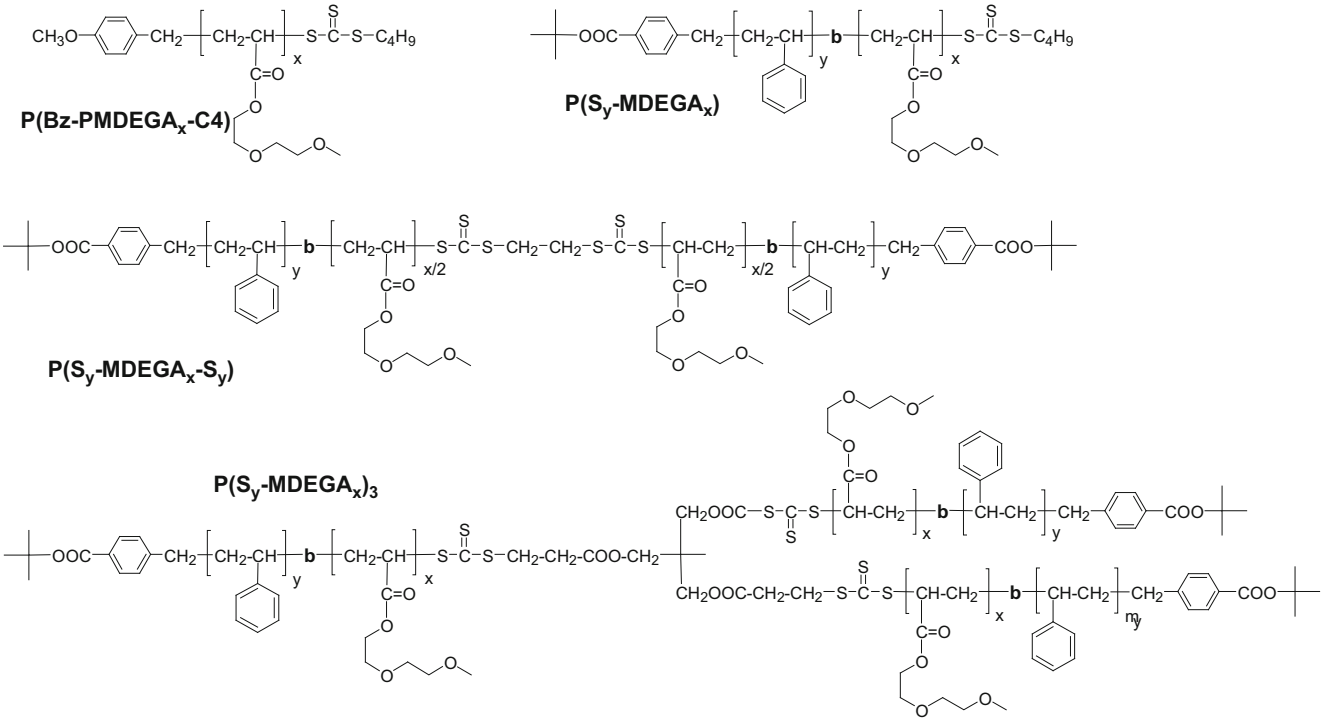

Fig. 2 General chemical structures of the synthesized polymers based on poly(methoxy diethylene glycol acrylate) **PMDEGA**

These extra H-bonds must be broken and the reorganization must be reversed when cooling the dispersions below the phase transition temperature. The PMDEGA chains, in contrast, cannot establish hydrogen bonds between themselves, and thus may react faster. These molecular differences may also contribute to the fact that PMDEGA-based polymers macroscopically phase-separate from their solutions when kept for some time above the cloud point. In contrast, PNIPAM-based polymers and micelles only aggregate to larger clusters with hydrodynamic diameters in the typical range of 100–500 nm, thus forming so-called mesoglobules [64, 66, 67].

Clearly, the detailed chemical nature of the thermo-responsive polymers is of extreme importance for their behavior in aqueous solution. Thus, the choice of a specific polymer for implementing supramolecular and responsive systems is not simply a matter of the exact value of the phase transition temperature. Moreover, the behavior of such systems cannot be ascribed and predicted by a simplified model considering just size, volume fraction and distribution of the various hydrophilic and hydrophobic polymer fragments within the macromolecules, based just on general architectural patterns as shown in Scheme 1.

The dilute and concentrated aqueous solutions/dispersions of the copolymers are clear to the naked eye at 20 °C. However, as evident from dynamic light scattering studies, the copolymers form aggregates already in highly dilute aqueous solution with hydrodynamic diameters typically in the range of 5–50 nm, as would have been expected according to their amphiphilic structures. Thus, we can assume that they form micelle-like structures, with a hydrophobic core made of the various B blocks, and a hydrophilic corona made of the thermo-responsive A blocks. A more detailed discussion of the aggregate structures is given further below.

Hydrogel Formation

Different from the homopolymers PNIPAM and PMDEGA, the aqueous solutions of the amphiphilic blocks copolymers become highly viscous with increasing concentration and eventually gel [24, 25]. The efficiency of gel formation as well as the shape of the phase diagrams may vary strongly not only with the relative and absolute sizes of the various hydrophilic and hydrophobic polymer blocks contained, but also with the architectures, i.e., whether diblock, triblock or star block copolymers are used (cf. Scheme 1). This is exemplified in Table 3 and Fig. 5. In the case of PMDEGA serving as thermo-responsive hydrophilic block, it is evident that the efficiency of hydrogel formation increases from the BA diblock via the BAB triblock to the star block structure. Further, for a given size of the hydrophobic block, hydrogel formation is favored by increasing the length of the hydrophilic block. An increase of the size of the hydrophobic PS blocks favors hydrogel formation, too, yet

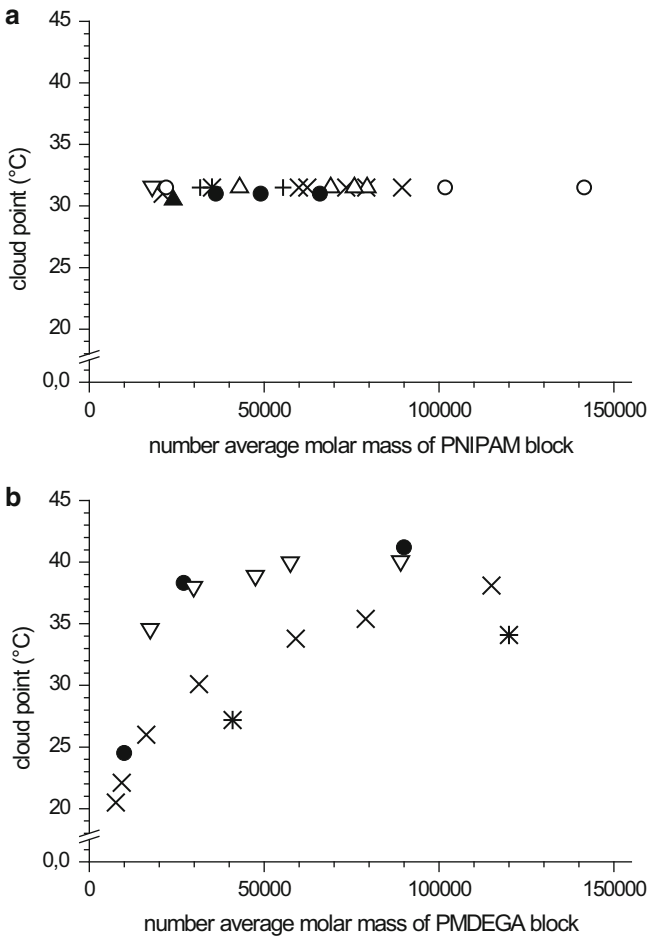

Fig. 3 Comparison of the LCST-type behavior of amphiphilic block copolymers of different structures and architectures in dilute aqueous solution, in dependence on the nature and absolute length of the thermo-responsive block (data from refs. [24, 25, 41, 42]). (**a**) **PNIPAM**-based polymers: (•) homopolymer; (∇) BA diblock copolymers with B = **PS**; (×) BAB triblock copolymers with B = **PS**; (+) BAB triblock copolymers with B = **PtbS**; (✳) BAB triblock copolymers with B = **DBBA**; (Δ) BAB triblock series with B = **PEHA**; (O) BAB triblock series with B = **PODA** (variable size of the B blocks, 1.0 g L^{-1} polymer in water, heating rate 1 °C min^{-1}). (**b**) **PMDEGA**-based polymers: (•) homopolymer (using RAFT agent 1,2-bis[4-(*tert*-butoxycarbonyl)benzyl sulfanylthiocarbonyl sulfanyl] ethane); (∇) BA diblock copolymers with B = $\mathbf{PS_{11}}$; (×) BAB triblock copolymers with B = $\mathbf{PS_8}$; (✳) $(BA)_3$ 3-arm star block copolymers with B = $\mathbf{PS_8}$ (3.0 g L^{-1} polymer in water, heating rate 1 °C min^{-1})

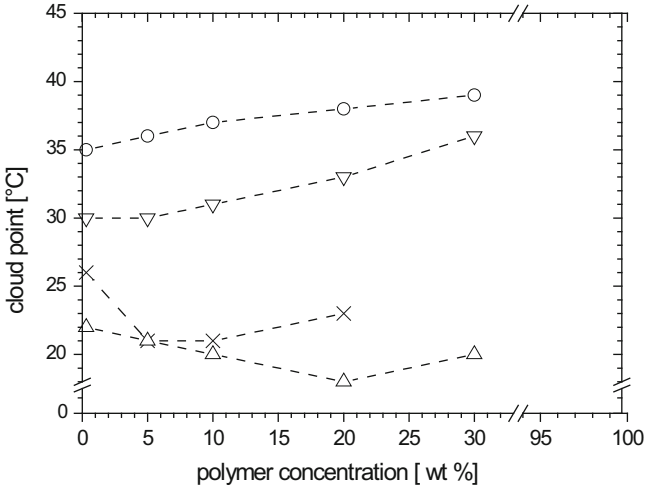

Fig. 4 Evolution of the cloud point temperatures of aqueous solutions of $\mathbf{P(S_8\text{-}MDEGA_n\text{-}S_8)}$ block copolymers with concentration: (O) $\mathbf{P(S_8\text{-}MDEGA_{452}\text{-}S_8)}$, (∇) $\mathbf{P(S_8\text{-}MDEGA_{180}\text{-}S_8)}$, (×) $\mathbf{P(S_8\text{-}MDEGA_{93}\text{-}S_8)}$ and (Δ) $\mathbf{P(S_8\text{-}MDEGA_{53}\text{-}S_8)}$ (Data taken from ref. [25]. Broken lines are meant as guide to the eye)

the direct solubility in water rapidly dwindles with increasing the hydrophobic blocks' size. While copolymers with $\mathbf{PS_{11}}$ blocks (at least according to visual inspection) can still fully dissolve in water, copolymers with $\mathbf{PS_{15}}$ blocks do not dissolve anymore, at least not within practical time scales. Hence, for such copolymers an indirect dispersion process must be applied, *e.g.*, dissolution in a water-miscible organic solvent, dilution by excess water, subsequent removal of the organic cosolvent, and adjustment to the desired concentration [24]. We also observe that BAB block copolymers with relatively short PMDEGA blocks, as in $\mathbf{P(S_8\text{-}MDEGA_{53}\text{-}S_8)}$, form biphasic systems in water [25]. This may be correlated with the general phase diagram of hydrophobically modified telechelics [15], which are employed as associative thickeners, indicating the formation of aggregates even at high dilution. When the average polymer chain length becomes smaller than the average intermicellar distance in the dynamic network, phase separation into a viscous concentrated and a dilute low-viscous phase occurs that is driven by entropy. Characteristically for the PMDEGA-based systems, we observe that, for a given concentration, the tendency for hydrogel formation decreases markedly with increasing temperature, and, when the gel–sol borderline is reached, the hydrogels disintegrate. This can occur much below the LCST-type phase transition temperature of the thermo-responsive block, giving rise to phase diagrams of versatile shape and in a sensitive dependence on the precise molecular structure (cf. Fig. 5) [25].

While the general correlation rules between the molecular structure and the gelling behavior as discussed above for the PMDEGA-based systems might intuitively seem logical for amphiphilic block copolymers, the PNIPAM-based systems behave completely differently. It is not only in their thermo-responsive behavior, as visualized by the cloud point lines in Fig. 5, where PMDEGA- and the PNIPAM-based systems show fundamental differences. The very weak dependence of hydrogel formation on the molecular structure of PNIPAM-based block copolymers seems as characteristic for these systems as it is striking. In fact, only one partial phase diagram of a PNIPAM-based block copolymer is displayed in Fig. 5, as the differences between all the block copolymers listed in Table 1 have been shown to be small at best [24].

Table 3 Hydrogel formation as function of **PMDEGA**-based block copolymer architecture and relative sizes of the hydrophilic and hydrophobic blocks at 21 °C, according to tube inversion tests. Data taken from refs. [25, 41, 61]

Polymer	Architecture	5 wt%	10 wt%	20 wt%	30 wt%
$PMDEGA_{513}$	Homopolymer	L	L	L	L
$P(S_{11}\text{-}MDEGA_{172})$	BA diblock	L	L	L	VL
$P(S_{11}\text{-}MDEGA_{275})$	BA diblock	L	L	L	VL
$P(S_8\text{-}MDEGA_{53}\text{-}S_8)$	BAB triblock	Biphasic	Biphasic	Biphasic	Biphasic
$P(S_8\text{-}MDEGA_{93}\text{-}S_8)$	BAB triblock	L	L	VL	Soft gel
$P(S_8\text{-}MDEGA_{172}\text{-}S_8)$	BAB triblock	L	VL	Soft gel	Hard gel
$P(S_8\text{-}MDEGA_{452}\text{-}S_8)$	BAB triblock	VL	Soft gel	Hard gel	Hard gel
$P(S_{15}\text{-}MDEGA_{549}\text{-}S_{15})$	BAB triblock	Hard gel	Hard gel	Hard gel	Hard gel
$P(MDEGA_{231}\text{-}S_8)_{3x}$	$(BA)_{3x}$ star block	VL	Soft gel	Hard gel	Hard gel

L free flowing liquid, *VL* viscous liquid

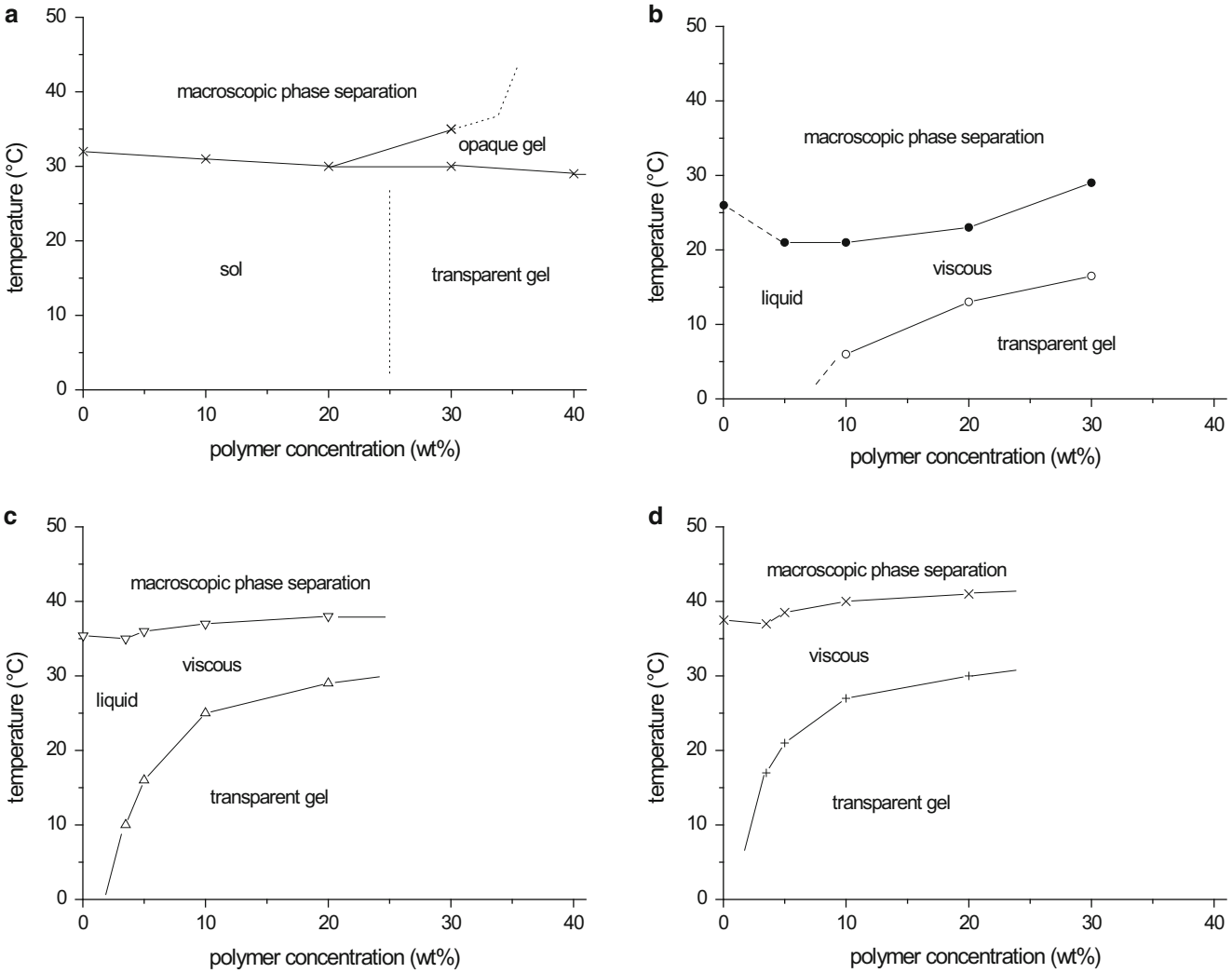

Fig. 5 Partial phase diagrams of amphiphilic BAB triblock copolymers in water. (**a**) **$P(S_{24}\text{-}NIPAM_{550}\text{-}S_{24})$**, (**b**) **$P(S_8\text{-}MDEGA_{93}\text{-}S_8)$.** (**c**) **$P(S_8\text{-}MDEGA_{452}\text{-}S_8)$.** (**d**) **$P(MDEGA_{231}\text{-}S_8)_{3x}$** (Data taken from refs. [24, 25, 61])

Depending on the detailed length of the PNIPAM-block, and on the size and chemical nature of the hydrophobic block(s), the necessary minimum concentration for gelling varies somewhat. But otherwise, the shapes of the diagrams are virtually the same for all types and lengths of the hydrophobic blocks studied, and for all studied lengths of the PNIPAM-block. Moreover, if a concentration is reached that suffices to induce hydrogel formation at low temperature, the

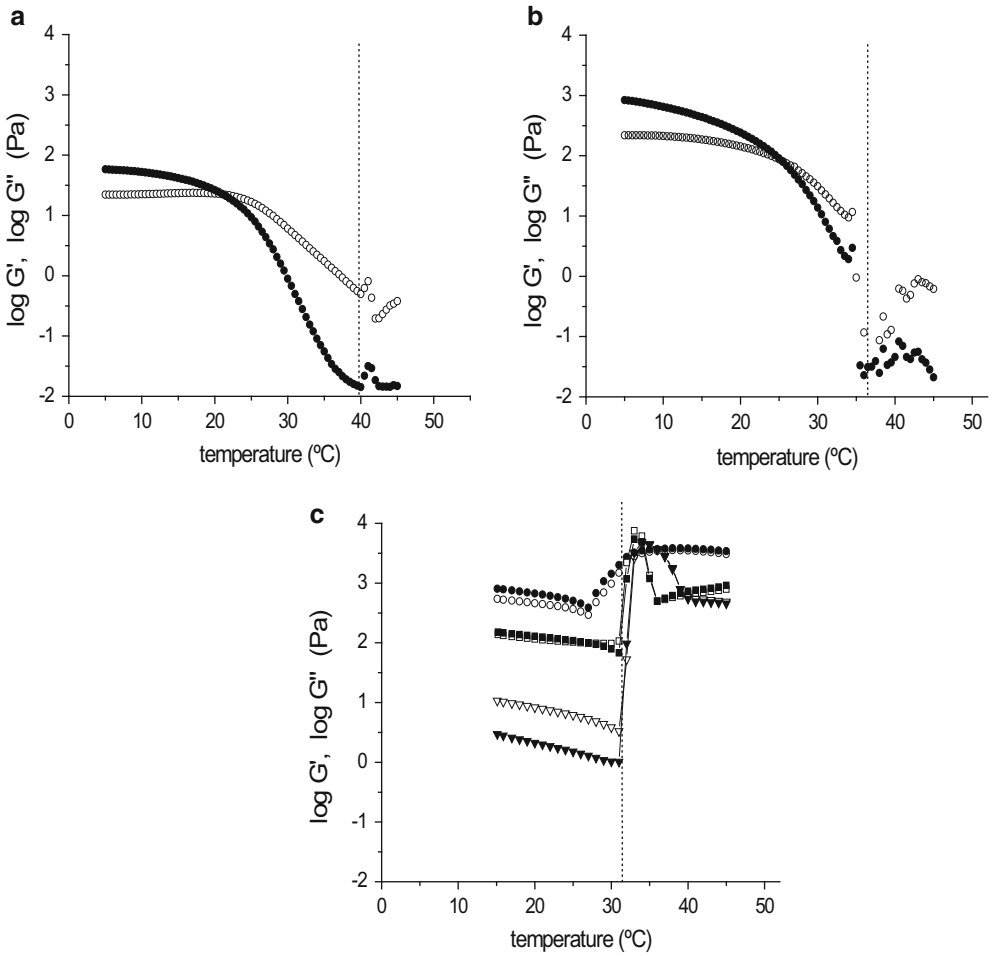

Fig. 6 Evolution of the storage (*full symbols*) and loss (*open symbols*) modulus of aqueous solutions of amphiphilic BA and BAB triblock copolymers with the temperature upon heating. (**a**) **P(S_{10}-MDEGA$_{450}$)** at 30 wt%; (**b**) **P(S_8-MDEGA$_{452}$-S_8)** at 10 wt%; (**c**) **P(S_{24}-NIPAM$_{550}$-S_{24})** at 20 (▼, ▽), 30 (■, □) and 40 wt% (●, ○).*Vertical dotted lines* indicate the position of the phase transition according to turbidimetry (Data taken from refs. [24, 25, 61])

gel state persists up to the cloud point of the PNIPAM-block. Even more strikingly for intermediate polymer concentrations of 20–30 wt%, the thermal collapse of the hydrophilic block apparently enhances the ability for gelling, instead of causing a breakdown of the hydrogels (cf. Fig. 5), at least for quite some temperature window of 5–10 °C above the cloud point (for a putative explanation of this phenomenon, see discussion of Fig. 6 below).

These qualitative findings concerning hydrogel formation are corroborated and can be refined by rheological studies. The characteristic, differing behaviors of the PMDEGA- and the PNIPAM-based copolymers are illustrated in Fig. 6. Clearly, the BAB triblock copolymers are much better suited to form gels than BA diblock copolymer analogs (criterion: storage modulus $G' >$ loss modulus G''). The comparison of Fig. 6 exemplifies that even at much higher concentrations, the gel–sol transition temperature of a diblock copolymer **P(S_y-MDEGA$_x$)** occurs already at lower temperatures than for the analogous BAB triblock copolymer **P(S_y-MDEGA$_x$-S_y)** despite the similar lengths of the hydrophobic as well as of the hydrophilic block. Also, the hydrogels formed by the diblock copolymer are mechanically much weaker, i.e., G'(diblock) < G'(triblock). Furthermore, Fig. 6 illustrates that the PMDEGA-based triblock copolymers can form hydrogels already at rather low concentrations (10 wt% and less, see Fig. 6), while PNIPAM-based copolymers of comparable architecture require much higher concentrations for gelation (Fig. 6). Regarding the examples displayed in Fig. 6 for instance, gel formation occurs only from about 30 wt% solutions on, though both the sizes of the PS-blocks and of the hydrophilic block are much bigger than in the analogous PMDEGA-based triblock copolymer.

Even more distinct, however, is the evolution of the moduli with temperature: The strength of the gel of the PMDEGA-based copolymer continuously weakens with

temperature until the gel point is crossed and G' gets smaller than G'', and finally, the viscosifying effect virtually disappears above the cloud point (Fig. 6). In strong contrast, the thermal softening of the gels is not only much weaker for PNIPAM-based copolymers, but the hydrogels are strongly reinforced when passing through the cloud point (Fig. 6). This suggests the existence of balanced attractive interactions between the collapsing PNIPAM-shells of the block copolymer aggregates (see below), which may be at least in parts explained by the intermolecular H-bonds formed between different PNIPAM-chains following the collapse transition. This explanation is supported by the fact that similar to the turbidimetry studies in dilute solution, we observe strong hysteresis for the rheological behavior of the PNIPAM-based copolymers during heating and cooling cycles, while this is much less the case for PMDEGA-based copolymers [24, 25, 41].

Aggregation and Segmental Dynamics in Solution

The transition behavior of diblock copolymers **P(S-NIPAM)** and triblock copolymers **P(S-NIPAM-S)** and **P(S-MDEGA-S)** is mainly determined by the chain architecture: The absence or presence of bridging between micelles seems to be the most important feature. For instance, the collapse and aggregation behavior at the cloud point is shown in Fig. 7. A diblock copolymer with a short PS block and a long PNIPAM block was chosen which is expected to form spherical micelles. Diblock copolymers **P(S_{50}-NIPAM$_{160}$)** form micelles in dilute aqueous solutions which shrink slightly as temperature is increased towards the cloud point (Fig. 7). At the cloud point, their hydrodynamic radius decreases drastically, i.e., the micellar shell has collapsed. At higher temperatures, large aggregates ("clusters") are observed which, interestingly, are stable in size at 80 nm. Two triblock copolymers **P(d8S_{10}-NIPAM$_{390}$-d8S_{10})** and **P(S_8-MDEGA$_{452}$-S_8)** having very short PS block as well as thermoresponsive blocks which are approximately twice as long as the ones of the **P(S_{50}-NIPAM$_{160}$)** diblock copolymer were chosen for comparison. In contrast to the diblock copolymer, both triblock copolymers immediately form large clusters at the cloud point, and single collapsed micelles cannot be observed (Fig. 7). The cluster size depends on the nature of the thermo-responsive block: For **P(d8S_{10}-NIPAM$_{390}$-d8S_{10})**, the size is ∼70 nm, i.e., similar to the diblock copolymer (Fig. 7), whereas the ones in **P(S_8-MDEGA$_{452}$-S_8)** are much bigger with ∼1000 nm in radius. We assume that PNIPAM becomes glassy when water is released (dry $T_g = 133$ °C [68]), which hampers the growth of the clusters, in agreement with the literature [64]. In contrast, PMDEGA (dry $T_g < -40$ °C) stays liquid-like, enabling the growth of very large clusters. In all cases, the micellar structure is preserved in the clusters [25, 44, 46].

All copolymers studied form spherical core-shell micelles in aqueous solution: star-like micelles for **P(S-NIPAM)** diblock copolymers and flower-like micelles with a certain degree of bridging for **P(S-NIPAM-S)** and **P(S-MDEGA-S)** triblock copolymers [25, 44, 46]. Small-angle neutron scattering (SANS) on concentrated solutions revealed that diblock copolymer **P(S_{50}-NIPAM$_{160}$)** forms core-shell micelles with a peculiar behavior around the cloud point (Fig. 8) [46]: The micellar radius increases towards the cloud point and shows critical behavior, whereas the core radius is relatively constant, as expected. Thus, the micellar shell swells as the cloud point is increased; we attribute this behavior to the release of water from the shell and the transient formation of a dry brush which is thicker than a wet brush. Interestingly, the micellar radius decreases only gradually over a broad temperature region. The correlation between the micelles is liquid-like and is described by the hard-sphere radius – basically half the distance between the centers of the micellar cores – and the volume fraction η, i.e., the packing density of the micelles. For the **P(S_{50}-NIPAM$_{160}$)** diblock copolymer, η decreases as the cloud point is approached, i.e. the interaction between them becomes weaker, but above the cloud point, it increases again when the clusters of collapsed micelles form. The transition region is relatively broad, which we attribute to the absence of bridging between the micelles. The star-like micelles gradually form larger and larger clusters as the temperature is increased above the cloud point.

For the triblock copolymer **P(d8S_{10}-NIPAM$_{390}$-d8S_{10})** at 220 g L^{-1} in D_2O, the micellar and the hard-sphere radius are quite constant below the cloud point, and decrease abruptly at the cloud point (Fig. 8). The core-shell structure is preserved in the collapsed state. The volume fraction behaves similarly to the one of the diblock copolymer. These micelles made from BAB triblock copolymers are already partially bridged below the cloud point, and the collapse of the PNIPAM blocks leads to an abrupt collapse of the shell and the mutual distance. In time-resolved SANS measurements during a temperature jump across the cloud point [47, 48], pre-transitional fluctuations in a narrow region below the cloud point could be resolved: Already below the cloud point, the correlation between the micelles decreases, and the formation of aggregates is a complex multi-step process (not shown).

The triblock copolymer **P(S_8-MDEGA$_{452}$-S_8)** behaves differently: No core-shell structure could be detected. Instead, the micelles could be described as homogeneous spheres with small scale fluctuation reflecting the structure of the shell. The micellar radius increases as the temperature is raised above the cloud point and then decreases slightly,

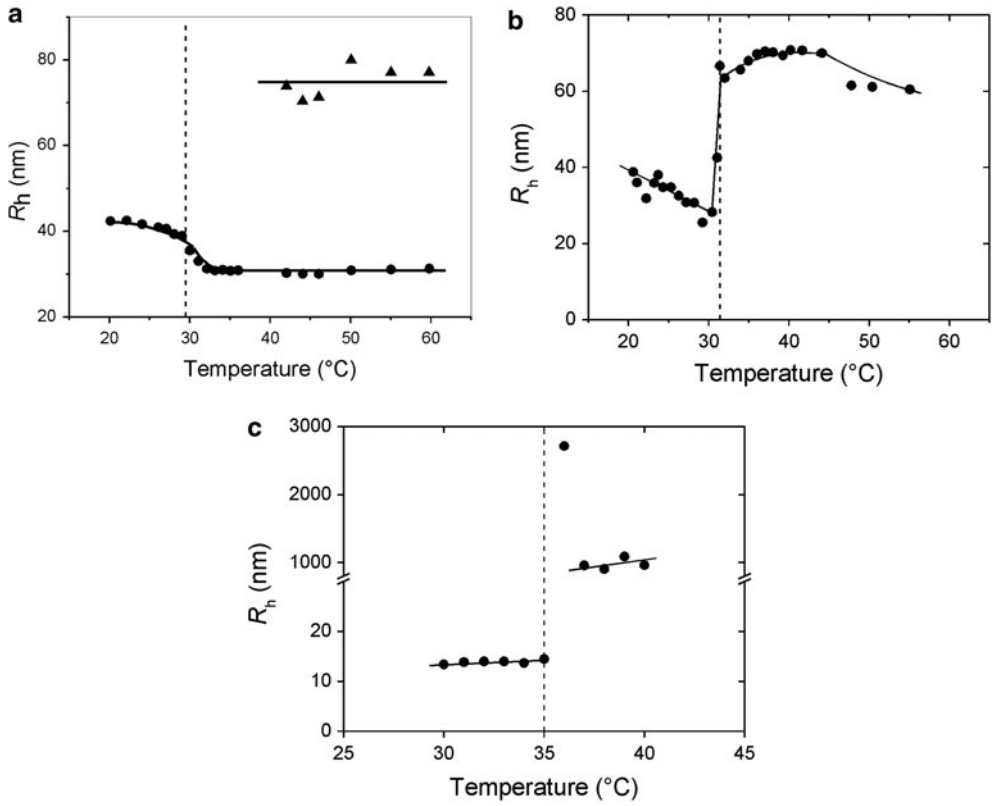

Fig. 7 Hydrodynamic radii of aqueous solutions (**a**) **P(S_{50}-NIPAM$_{160}$)** at 0.20 g L^{-1} [42], (**b**) **P(d8S_{10}-NIPAM$_{390}$-d8S_{10})** at 0.20 g L^{-1} [44], and (**c**) **P(S_8-MDEGA$_{452}$-PS_8)** at 3.0 g L^{-1} [25] as determined using dynamic light scattering. Heating runs

i.e., no abrupt decrease is observed as in the PNIPAM based systems (Fig. 8). The hard-sphere radius decreases smoothly in the entire temperature range studied without any discontinuity at the cloud point. The only drastic change at the cloud point is the steep minimum of the volume fraction: Again, the correlation between micelles gets gradually lost as the cloud point is approached, but is reinstalled in the collapsed state. Clearly, there are several striking differences of the **P(S_8-MDEGA$_{452}$-PS_8)** system with respect to the **P(d8S_{10}-NIPAM$_{390}$-d8S_{10})** system, which reflect the different chemical nature of the thermo-responsive block. Changes may also be due to the length of the PS block which possibly passes some critical limit between 8 and 10 monomers. Scheme 2 summarizes the behavior observed for the three systems.

Neutron spin-echo spectroscopy revealed a number of dynamic processes in concentrated solutions of **P(S_{50}-NIPAM$_{160}$)** and **P(d8S_{10}-NIPAM$_{390}$-d8S_{10})** below the cloud point: the segmental dynamics of PS (in case of protonated PS), the so-called breathing mode of PNIPAM, i.e., the collective dynamics of the swollen PNIPAM shell, and the diffusion of entire micelles (Fig. 9) [44, 46]. The different relative block lengths together with the two architectures (star-like and flower-like micelles) allowed us to vary the grafting density of PNIPAM blocks at the surface of the PS core between 0.20 nm^{-2} and 0.61 nm^{-2}. These values were deduced from the core sizes found in SANS measurements. For both grafting densities, the breathing mode was dominant over the single-chain Zimm dynamics, which is consistent with other studies [69, 70]. With increasing polymer concentration, the segmental mode of the PNIPAM block becomes slower, as expected. Similar findings are made with **P(d8S_{10}-NIPAM$_{390}$-d8S_{10})**, but in the swollen state, the segmental mode of the PNIPAM block is slower than in the diblock. We attribute this difference to the back folding of the PNIPAM block into the same micellar core, or to the bridging of two micelles.

Interestingly, for both systems, the segmental dynamics in the collapsed state are independent of polymer concentration and faster than in the swollen state. We attribute this finding to a "freezing in" of the segmental dynamics of the PNIPAM shell except a few strands that stick out into the solution.

The segmental dynamics thus reflects the micellar architecture: Because of the relatively high grafting density of shell blocks on the core surface, the breathing mode of the shell blocks dominates and is influenced by back folding and bridging.

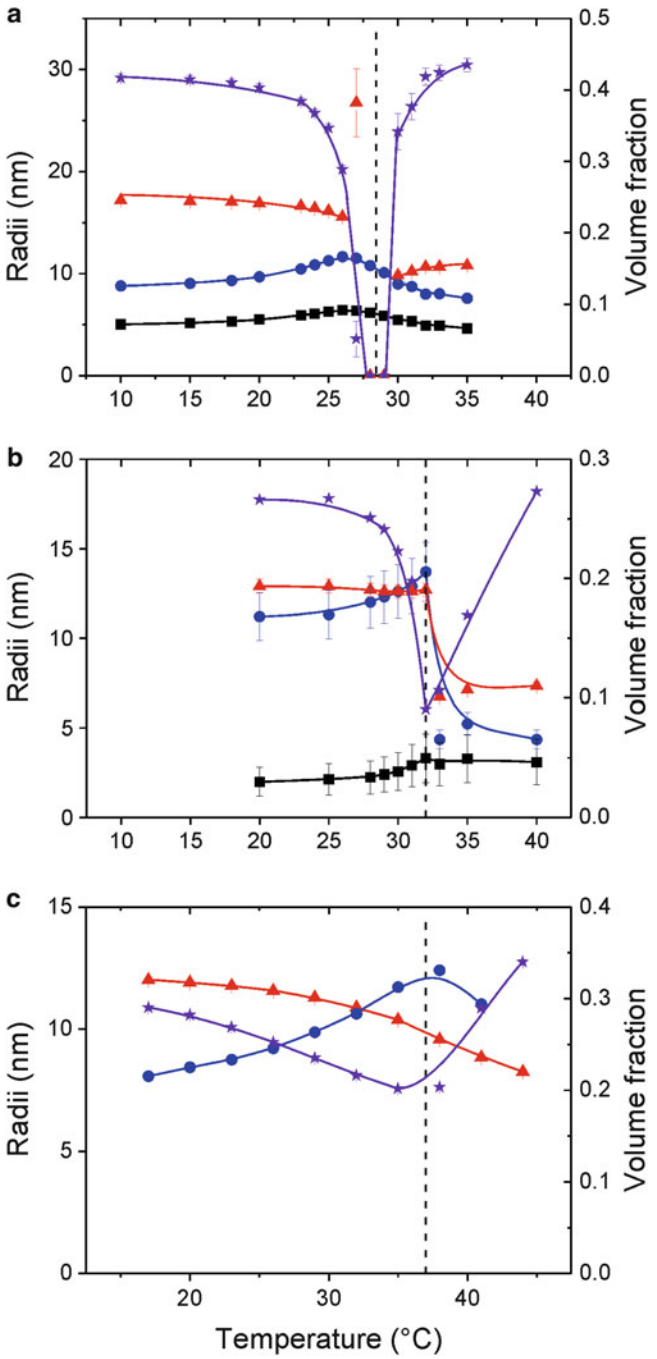

Fig. 8 Micellar dimensions as determined using SANS. (**a**) **P(S_{50}-NIPAM$_{160}$)** at 470 g L^{-1} in D_2O [46]. (**b**) **P(d8S_{10}-NIPAM$_{390}$-d8S_{10})** at 220 g L^{-1} in D_2O [44], and (**c**) **P(S_8-MDEGA$_{452}$-S_8)** at 10 wt.% in H_2O [25]. *Filled squares*: core radius, *filled circles*: micellar radius, *filled triangles up*: hard-sphere radius (*all left axis*); *stars*: volume fraction (*right axis*). *Dashed lines*: cloud points

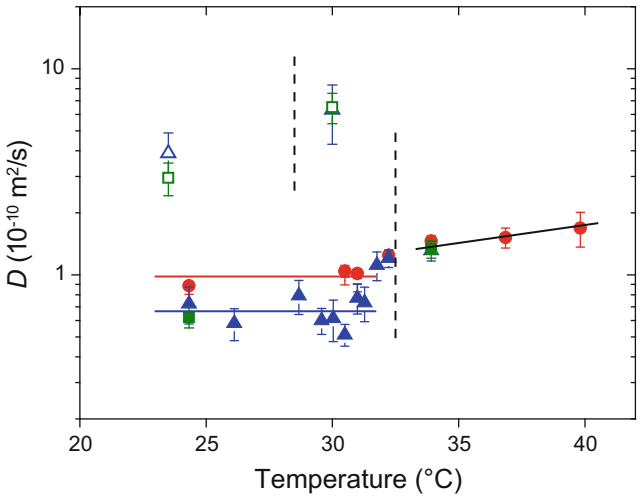

Fig. 9 Temperature-dependence of the diffusion coefficients of the segmental dynamics of the PNIPAM block. Open symbols: **P(S_{50}-NIPAM$_{160}$)** [46], *closed symbols*: **P(d8S_{10}-NIPAM$_{390}$-d8S_{10})** [44], both in D_2O. *Circles*: 50 g L^{-1}, *triangles up*: 200 g L^{-1}, *squares*: 300 g L^{-1}. The *dashed lines* indicate the respective cloud points

The studies of the bulk behavior have thus revealed a number of differences between **P(S-NIPAM)**, **P(S-NIPAM-S)** and **P(S-MDEGA-S)**, concerning the transition temperature, the width and hysteresis of the transition, the temperature-dependent mechanical properties, the collapse and aggregation behavior of micellar solutions and the segmental dynamics. Beyond the behavior in bulk solutions, complementary investigations on thin films attracted our interest as well, because many potential applications of such "smart" hydrogels, for instance in sensors, switches or valves, require their use as (thin) films. Of fundamental interest are questions related to methods for the preparation of homogeneous films, the stability of thin films, the interaction of the thermo-responsive block copolymers with the substrate, confinement effects imposed by the thin film geometry, anisotropic response such as uniaxial vs. three-dimensional swelling, and – more general – the structural rearrangements during swelling and collapse at the cloud point. Compared to the bulk studies, the thin film geometry offers the possibility to control the degree of swelling by using water vapor atmosphere, to determine the water content and the film thickness independently, and to distinguish lateral structural changes from those along the film normal. The next sections describe accordingly the structure of thin thermo-responsive films, their swelling and collapse transition as well as switching kinetics.

Thin Films

Thin thermo-responsive films of homopolymer **PNIPAM**, **PNIPAM** end-capped with *n*-butyltrithiocarbonate at both ends (**nbc-PNIPAM$_{340}$**) [55, 56, 71], amphiphilic diblock copolymers **P(S-NIPAM)** [72, 73] as well as triblock copolymers **P(S-NIPAM-S)** were prepared and studied on flat, smooth silicon supports. Analogous experiments

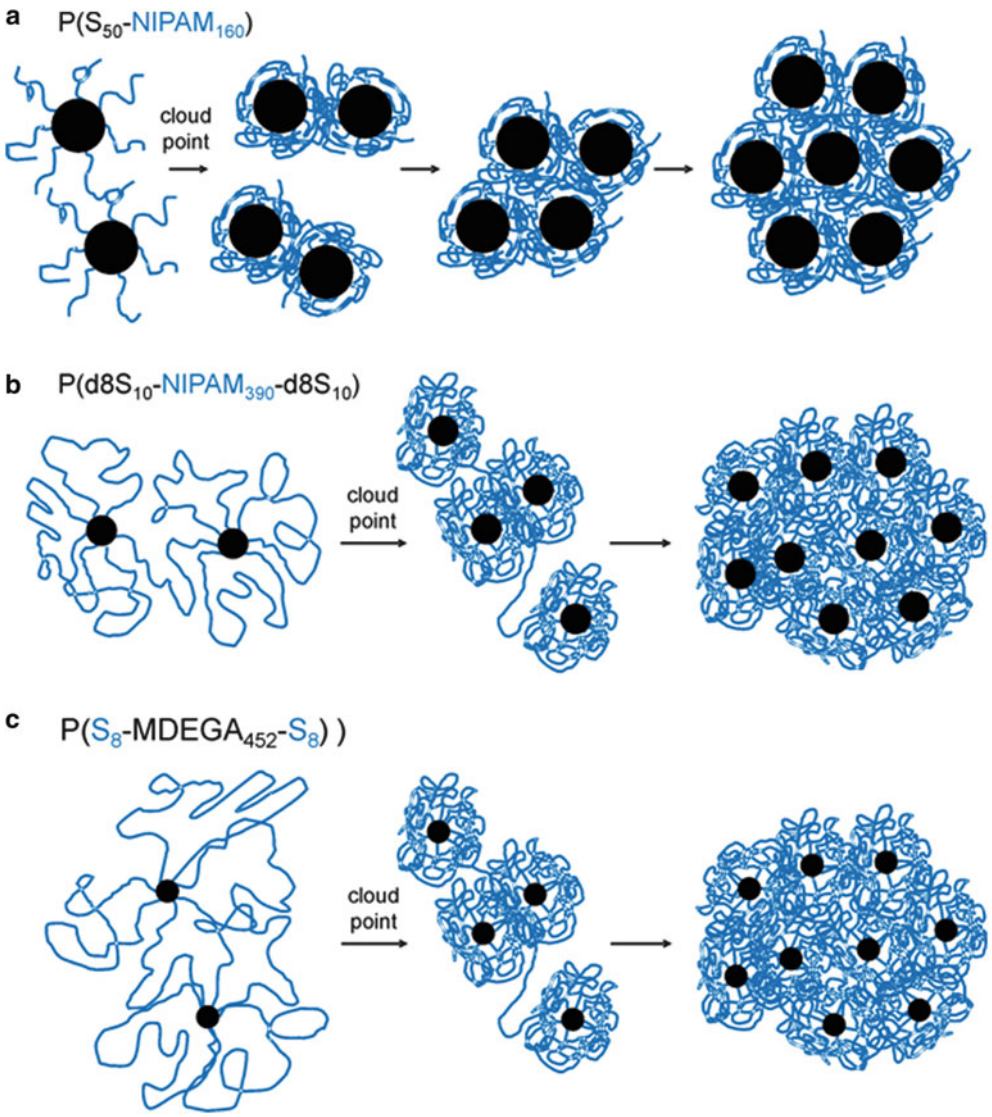

Scheme 2 Model of the phase behavior of the three systems studied in solution. For simplicity, the micellar cores of PS are sketched as homogeneous *circles*. The *blue lines* denote the thermo-responsive PNIPAM or PMDEGA blocks

were performed with homopolymer **PMDEGA** [57, 58] and the amphiphilic triblock copolymers **P(S-MDEGA-S)** [59, 60]. By spin coating on pre-cleaned substrates, smooth and homogeneous films are obtained as characterized by optical microscopy, atomic force microscopy (AFM) and X-ray reflectivity (XRR), whereas it was reported that very thick and bulk-like **PNIPAM** gel films (thicknesses on the order of 60 μm) were inhomogeneous on a micrometer scale [74]. In combination with the described substrate cleaning protocol, spin-coating from dioxane solutions turned out to result in the smoothest and most homogeneous films as compared to other solvents, *e.g.* water. No large aggregates were present in these solutions. Film thicknesses and polymer concentrations of the solution used in spin coating were found to correlate linearly for all polymers studied (see Fig. 10). This enables precise tailoring of the film thickness in a simple way for all the investigated thermo-responsive polymers, and thus, the film thickness was varied from nanometers to hundreds of nanometers. Figure 10 exemplifies XRR measurements of **nbc-PNIPAM$_{340}$** films. From the fit to the data, the density profile along the surface normal of these initially prepared films is extracted. It shows the enrichment of PNIPAM chains at the hydrophilic substrate. Thus the interaction with the substrate influences the arrangement of the polymer chains with respect to the substrate.

Using grazing-incidence small-angle X-ray scattering (GISAXS), the inner film morphology as well as long-ranged correlations in the films have been investigated. With respect to the inner film morphology, it turned out that already the very short *n*-butyltrithiocarbonate end groups of **nbc-**

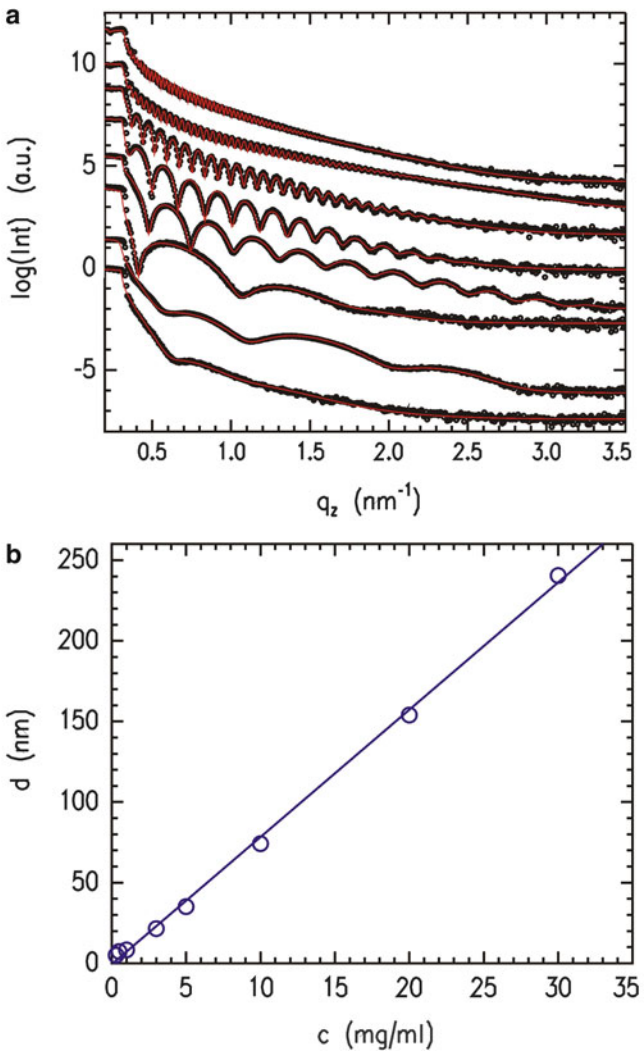

Fig. 10 Characterization of thermo-responsive hydrogel films of **nbc-PNIPAM$_{340}$** spin-coated from dioxane at room temperature and ambient conditions: (**a**) Representative XRR data (*dots*) shown together with model fits (*lines*) for the thickness regime covered in this investigation. With increasing film thickness (5, 7, 8, 22, 35, 74, 154 and 241 nm from *bottom* to *top*), the curves are shifted along the y-axis for presentation. (**b**) Film thickness d plotted as a function of the polymer concentration in the solution used for spin-coating. The *solid line* is a linear fit. (Reprinted with permission from Macromolecules 41, 3209–3218, 2008. Copyright (2008) American Chemical Society)

PNIPAM$_{340}$ can be regarded as miniaturized hydrophobic blocks of a BAB-type block copolymer (B denoting a hydrophobic and A a thermo-sensitive block), because an internal structure has been found [55]. Nevertheless, in case of diblock and triblock copolymers, *e.g.*, **P(S-NIPAM)**, **P(S-NIPAM-S)** and **P(S-MDEGA-S)**, the inner morphology of the analogously prepared spin-coated films is much better defined, due to an increase in long-ranged order, and a well established micro-phase separation structure is observed [57–60, 72, 73] In case of **PNIPAM** films, correlated roughness is observed [55]. Thus the surface of the thermo-responsive film is partly correlated with the surface of the underlying substrate, meaning that the roughness spectrum of the substrate is transferred through the polymer film. In contrast, **PMDEGA** based films do not have this spatial correlations. Hence, such correlations are absent and both roughness spectra are independent [57, 60]. This difference between **PNIPAM** and **PMDEGA** films is attributed to the very different glass transition temperatures T_g of both polymers. Due to the high value of T_g(PNIPAM) of about 133 °C, the surface structure installed during spin coating is frozen-in. Very similar to the behavior of other glassy homopolymers such as for example polystyrene [75, 76], the liquid surface couples to the roughness spectrum of the substrate, and the **PNIPAM** chains have no possibility to relax into an energetically more favorable state. In contrast, the low value of T_g(PMDEGA) of < -40 °C gives sufficient mobility to the **PMDEGA** chains to rearrange after spin coating and to erase the correlated roughness. In fact, due to the mobility of the PMDEGA chains, the films roughen during storage under ambient conditions as measured with optical microscopy and AFM. An onset of dewetting is visible already after 1 day, and holes of different diameter are found on the films' surfaces [57].

Thin Film Swelling and Collapse Transition

From the various polymers studied in bulk solution and hydrogels (Tables 1 and 2), we chose **nbc-PNIPAM$_{340}$**, **P(S$_{50}$-NIPAM$_{160}$)**, **PMDEGA$_{138}$** and **P(S$_{11}$-MDEGA$_{126}$-S$_{11}$)** for closer inspection in thin films. The LCST-type transition from a swollen to a collapsed film has been studied for films exposed to water vapor atmosphere, where the degree of swelling is tuned via the humidity of the atmosphere surrounding the thermoresponsive films [58].

The swelling process of PNIPAM and PMDEGA films was monitored by in-situ neutron reflectivity, revealing two regimes (see Fig. 11). In the first regime, the film thickness remains constant and the water volume fraction increases rapidly, as water occupies all holes and vacancies of the polymer film given by the free volume of the film [71]. In the second regime, water is absorbed by the hydrophilic polymer chains, causing the film to swell, so that film thickness and water volume fraction increase slowly.

This second process can be described by a modified diffusion process using a model explaining gel swelling kinetics [77–79]. In this model, swelling (or shrinking) follows first-order kinetics, and is not considered as a pure diffusion process. Information about the thin thermoresponsive film such as shear modulus and osmotic modulus as well as the relaxation time of the swelling can be extracted from the model fit [56, 58, 72, 73]. The actual values for PNIPAM

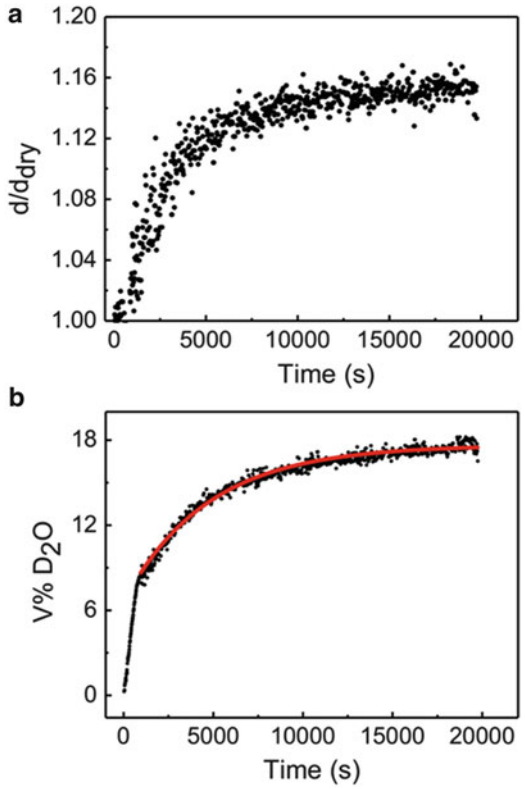

Fig. 11 Response of the **PMDEGA$_{138}$** film with thickness of 35.9 nm to swelling at 23 °C: (**a**) Relative film thickness and (**b**) D_2O volume fraction (V% D_2O) as a function of swelling time, and the *solid line* in (**b**) is a fit of a model as explained in the text (Soft Matter 8, 5241–5249 (2012) – Reproduced by permission of The Royal Society of Chemistry)

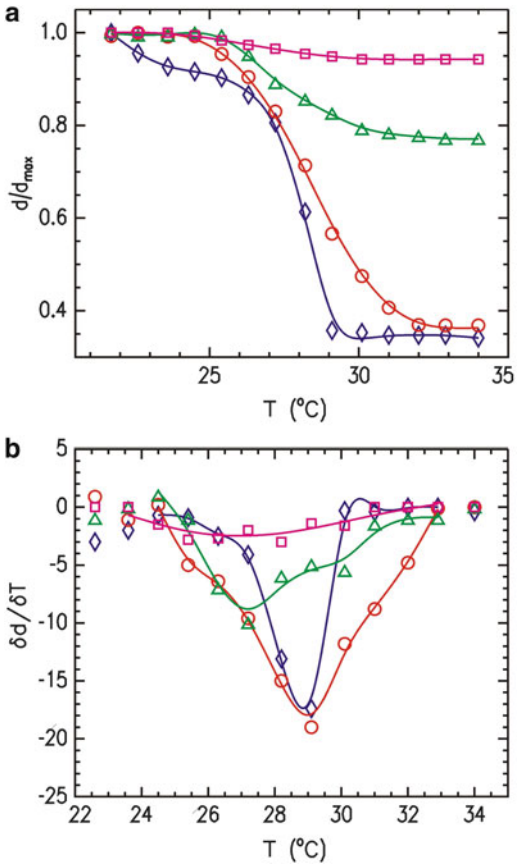

Fig. 12 (**a**) Temperature dependent changes of the film thickness measured for dry **nbc-PNIPAM$_{340}$** films exposed to saturated water vapor and (**b**) first derivative indicating the transition temperature and the width of the transition. The swelling curves are measured for film thickness of 10.5 (rhombs), 40 (*circles*), 105 (*triangles*) and 200 nm (*squares*). The *solid lines* are guides to the eye. (Reprinted with permission from Macromolecules 41, 3209–3218, 2008. Copyright (2008) American Chemical Society)

and PMDEGA films differ due to the different mechanical properties.

When monitoring the accompanying change in film thickness during swelling at a fixed temperature, an increasing swelling capacity is found for decreasing film thickness [55, 57]. In combination with the hydrophilic substrate surface, which favors the PNIPAM or PMDEGA segments as well as water, the swelling might be increased by a type of entropic spring change in the conformation of the polymers. With increasing film thickness, this effect gets weaker because fewer molecules are in a perturbed conformation [55]. In the literature, only a few swelling experiments for thin thermo-responsive hydrogel films have been reported, which mostly have focused on PNIPAM end-grafted on the substrates [80–83], thus a direct comparison of our results is difficult. For sure, the conformation of end-tethered PNIPAM in thin film geometry will differ from the one of non-covalently bound chains, which is our case.

In general, all investigated **PNIPAM** and **PMDEGA** films show a collapse transition upon heating. Figure 12 shows the example of the temperature dependent changes of the film thickness measured for **nbc-PNIPAM$_{340}$** films of different thickness [55]. As compared with the corresponding aqueous solution, the transition temperature is shifted to lower values. The transition temperature decreases with increasing hydrogel film thickness, demonstrating that even 200 nm thick films are not bulk-like and differ from solutions. In addition, the width of the transition increases with film thickness. The 10.5 nm thick **nbc-PNIPAM$_{340}$** film exhibits a very sharp transition within a temperature change of 2 °C, which is small as compared to bulk samples, while for 200 nm thick films, the observed transition width is equivalent to the bulk behavior [55]. Looking to the changes in more detail, it appears as if the transition at an intermediate film thickness of 105 nm occurs in two steps: one dominant step at the temperature as seen for thicker films and one less pronounced step at the temperature found for thinner films. Hence, thin films and the part of thicker films that is near to the substrate, are affected by the interaction with the underlying substrate.

PMDEGA films show the same characteristics of thermo-responsive behavior in thin films as PNIPAM-based poly-

mers: the transition temperatures are reduced in thin films as compared with solutions, and the transition temperatures decrease with increasing film thickness. However, compared to **PNIPAM** films, the width of the transition is increased. This difference in the width of the transition may be related to the different mechanisms of water release. In the case of **PNIPAM**, two types of bound water coexist [65, 84, 85]. The first type is bound by hydrogen bonds to the amide group, while the second type forms a water cage surrounding the hydrophobic moieties. When the temperature increases above the LCST-type transition temperature, both types of water are released from the film. According to the model of cooperative hydration of the **PNIPAM** chain, a pearl-necklace like chain conformation is present in hydrated PNIPAM due to the large hydrophobic isopropyl side groups [86–88]. This consecutive sequence is dehydrated as a whole, causing a sharp transition. In contrast, **PMDEGA** does not dispose of strongly polarized H-atoms, and thus does not contain strongly or weakly acidic protons. As a consequence, **PMDEGA** can act in H-bonds only as acceptor (due to the free electron pairs of oxygen in the ether groups), but not as donor. The ester groups (anchoring the oligoethyleneglycolethers to the polymer backbone) are very weak acceptors and are commonly not considered to be able to form H-bonds, in particular with water. Thus, no cooperative effect is present in **PMDEGA,** and the transition is significantly broader than for **PNIPAM**.

Noteworthy, inert metals such as gold can be deposited homogenously on top of such thin thermo-responsive hydrogel films, as shown, for instance, for **nbc-PNIPAM$_{340}$**. This gives access to applications such as sensors or nano-switches. The deposition of a metal contact on top of the thermoresponsive films does not affect their ability to switch from an extended to a collapsed chain conformation, and thus to change the film thickness from an initial thickness to a lower value [56].

Switching Kinetics in Thin Films

In-situ neutron reflectivity was applied for investigating the switching kinetics. The swollen thermo-responsive films were exposed to an abrupt change in the temperature (called temperature jump) from a start temperature below the phase transition, to a value above the transition. Such kinetic investigations were performed analogously for both **PNIPAM** and **PMDEGA** based films. The use of deuterated water gives the necessary contrast to follow the changes in water content and in film thickness. In all cases, a complex response of the thermo-responsive film to the change in temperature is observed. Film thickness and water volume fraction show a multi-step behavior.

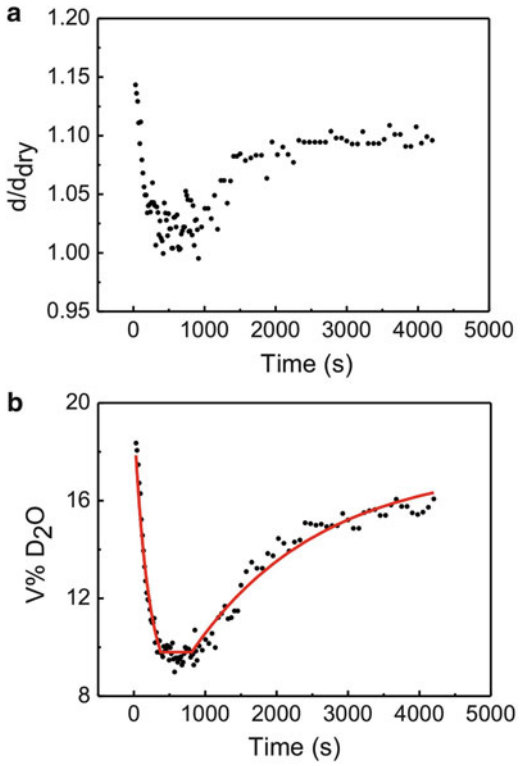

Fig. 13 Response of **PMDEGA$_{138}$** film with thickness of 35.9 nm to a temperature jump from 23 °C to 45 °C: (**a**) Relative film thickness and (**b**) D_2O volume fraction (V% D_2O) as a function of time. The *solid line* in (**b**) is a fit of a model as explained in the text (Soft Matter 8, 5241–5249 (2012) – Reproduced by permission of The Royal Society of Chemistry)

Figure 13 illustrates the example of **PMDEGA$_{138}$** hydrogel films [58]. The relative film thickness and the D_2O volume fraction (vol% D_2O) are plotted as a function of time t, with $t = 0$ being defined as the time at which the temperature is changed from 23 °C to 45 °C. The transition temperature is at 40 °C for the investigated film thickness of 35.9 nm. Three distinct regimes in the response are detected. The initial response of the **PMDEGA** film is fast (regime 1). The film reacts by decreasing the water content from 18 % to 9 %. The water release is accompanied by a shrinkage of the film back to its original dry thickness. The whole process takes only 400 s. When the film thickness is decreased to its initial value, a D_2O volume fraction of 9 % remains in the film. This residual water may occupy vacancies and holes in the porous **PMDEGA** film, which does not add to the film thickness (cf. discussion above), and is strongly bound to the polymer chains.

After the fast shrinkage event, film thickness and water volume fraction stay nearly constant for some time (regime 2). As the film is still located in the water vapor atmosphere after the collapse, the chains are assumed to slowly relax into a more favorable conformation. Due to this

rearrangement, the polymers are able to bind more water, and thus the films can reabsorb a certain amount of water. This results in an increase of film thickness (regime 3). Thus, the hydrogel film reacts with a complex three-stage process to the abrupt temperature jump.

When introducing an internal micro-phase separated structure, as for example in films of the amphiphilic triblock copolymers **P(S-MDEGA-S)** [60], or by adding a metal top layer [56], this general multi-stage process is not changed. In all cases, a response which can be understood as shrinkage, reorganization and reswelling is seen. In the case of thin thermo-responsive films based on **PNIPAM,** the duration of the reorganization step is only short. This again can be explained by the different type of hydrogen bonds formed by **PNIPAM** as compared with **PMDEGA**.

Conclusions

The methods of RDRP, in particular of RAFT polymerization, enabled us to prepare two families of amphiphilic thermo-responsive block copolymers, which vary systematically the chemical building blocks (i.e., nature and size of the hydrophilic, thermo-responsive as well as of the hydrophobic blocks), as well as the architecture the amphiphiles (homopolymer vs. diblock vs. symmetrical triblock *vs* star block copolymer). In particular we successfully fabricated two analogous polymer series based on PNIPAM and PMDEGA, respectively, as hydrophilic, thermo-sensitive "smart" blocks with a transition temperature in the biologically particularly interesting range of 30–40 °C.

For the characterization of bulk solutions and gels, the combination of a number of methods allowed us to investigate a large concentration range, ranging from below the critical micelle concentration to the highly concentrated regime. The temperature-dependent structural and dynamic properties of the solutions and gels could be characterized on a large range of length and time scales and could further the understanding of the macroscopic characteristics, such as the macroscopically observed phase behavior as well as the mechanical behavior. Kinetic measurements enabled us to follow the complex structural changes around the cloud point in great detail.

Thin films were successfully prepared on solid supports and investigated concerning film morphology, long range correlations, stability, swelling behavior and thermal response. X-ray and neutron scattering in combination with real space imaging techniques enabled us to follow the water incorporation as well as the chain collapse induced water release. The interaction with the substrate as well as confinement effects introduced by the film thickness turned out to influence the film structure as well as the film swelling.

In summary, the combination of modern synthesis methods, comprehensive solution, hydrogel and thin film studies with a number of different experimental methods allowed us to get a deeper understanding of the self-assembly as well as the collapse transition of this interesting system. This way, we could especially get an insight into the role of the chain architecture and the nature of the thermo-responsive block.

Acknowledgment The results presented are the outcome of combined research activities over a period of 6 years, which crucially depended on the creativity, labor, zeal and enthusiasm of many dedicated post-doctoral, Ph.D. and master students at Potsdam University and at TU München, who are (in alphabetical order) Joseph Adelsberger, C. Adrián Benítez-Montoya, Achille M. Bivigou-Koumba, Charles Darko, Alexander Diethert, Anastasia Golosova, Abhinav Jain, Gunar Kaune, Juliane Kristen, Amit Kulkarni, Andreas Meier-Koll, David Magerl, Ezzeldin Metwalli, Anna Miasnikova, Gabriele De Paoli, Monika Rawolle, Matthias A. Ruderer, Katja Skrabania, Kordelia Troll, Weinan Wang and Qi Zhong. Moreover, using large scale facilities, the approved beamtime and support by the beamline scientists (Peter Busch, Robert Cubitt, Sergio S. Funari, Isabelle Grillo, Olaf Holderer, Jan Perlich, Vitaliy Pipich, Stephan V. Roth) are acknowledged. Financial support was provided by Deutsche Forschungsgemeinschaft (DFG) via the priority program SPP 1259 "Intelligente Hydrogele" (grants LA611/7, MU1487/8 and PA771/4), by Fonds der Chemischen Industrie (FCI), and by German Academic Exchange Service (DAAD). In the priority program, we enjoyed fruitful collaboration with Regine von Klitzing (TU Berlin), Thomas Hellweg (Universität Bielefeld), Walter Richtering (RWTH Aachen), and Norbert Stock (Universität Kiel). Also, we gladly thank our external partners Franz Faupel (Universität Kiel), Eckhard Görnitz, Michael Päch (both Fraunhofer Institute for Applied Polymer Research, Potsdam), Marianne Hanzlik (Technische Universität München), Klaus Rätzke (Universität Kiel), Ralf Röhlsberger, and Kai Schlage (both DESY Hamburg) for their valuable input and support.

References

1. Kopeček J (2009) J Polym Sci, Part A: Polym Chem 47:5929–5946
2. Vlierberghe SV, Dubruel P, Schacht E (2011) Biomacromolecules 12:1387–1408
3. Wanka G, Hoffmann H, Ulbricht W (1994) Macromolecules 27:4145–4159
4. Mortensen K (2001) Coll Surf A 183–185:277–292
5. Hamley IW (2005) Block copolymers in solution: fundamentals and applications. Wiley, Chichester
6. Booth C, Attwood D (2000) Macromol Rapid Comm 21:501–527
7. Cohen Stuart MA (2008) Colloid Polym Sci 286:855–864
8. Kimerling AS, Rochefort WE, Bhatia SR (2006) Ind Eng Chem Res 45:6885–6889
9. Madsen J, Armes SP (2012) Soft Matter 8:592–605
10. Zhulina EB, Borisov OV (2012) Macromolecules 45:4429–4440
11. Halperin A (2006) J Macromol Sci C: Polym Rev 46:173–214
12. Tsitsilianis C, Iliopoulos I (2002) Macromolecules 35:3662–3667
13. Annable T, Buscall R, Ettelaie R, Whittlestone D (1993) J Rheol 37:695–726
14. Winnik MA, Yekta A (1997) Curr Opin Colloid Interface Sci 2:424–436
15. Chassenieux C, Nicolai T, Benyahia L (2011) Curr Opin Colloid Interface Sci 16:18–26
16. de Molina PM, Herfurth C, Laschewsky A, Gradzielski M (2011) Prog Colloid Polym Sci 138:67–72

17. Chaterji S, Kwon IK, Park K (2007) Prog Polym Sci 32:1083–1122
18. Tokarev I, Minko S (2009) Soft Matter 5:511–524
19. Liu R, Fraylich M, Saunders BR (2009) Colloid Polym Sci 287:627–643
20. Kratz K, Hellweg T, Eimer W (2000) Coll Surf A 170:137–149
21. Stieger M, Richtering W, Pedersen JS, Lindner P (2004) J Chem Phys 120:6197–6206
22. Dimitrov I, Trzebicka B, Müller AHE, Dworak A, Tsvetanov CB (2007) Prog Polym Sci 32:1275–1343
23. Tsitsilianis C (2010) Soft Matter 6:2372–2388
24. Bivigou-Koumba AM, Görnitz E, Laschewsky A, Müller-Buschbaum P, Papadakis CM (2010) Colloid Polym Sci 288:499–517
25. Miasnikova A, Laschewsky A, De Paoli G, Papadakis CM, Müller-Buschbaum P, Funari SS (2012) Langmuir 28:4479–4490
26. Taylor LD, Cerankowski LD (1975) J Polym Sci Part A: Polym Chem 13:2551–2570
27. Platé NA, Lebedeva TL, Valuev LI (1999) Polymer J Jpn 31:21–27
28. Schlaad H, Diehl C, Gress A, Meyer M, Demirel AL, Nur Y, Bertin A (2010) Macromol Rapid Comm 31:511–525
29. Schild HG (1992) Prog Polym Sci 17:163–249
30. Aseyev V, Tenhu H, Winnik F (2006) Adv Polym Sci 196:1–85
31. Aseyev V, Tenhu H, Winnik F (2011) Adv Polym Sci 242:29–89
32. Nykänen A, Nuopponen M, Laukkanen A, Hirvonen S-P, Rytelä M, Turanen O, Tenhu H, Mezzenga R, Ikkala O, Ruokolainen J (2007) Macromolecules 40:5827–5834
33. Zhou XC, Ye XD, Zhang GZ (2007) J Phys Chem B 111:5111–5115
34. Nykänen A, Nuopponen M, Hiekkataipale P, Hirvonen S-P, Soininen A, Tenhu H, Ikkala O, Mezzenga R, Ruokolainen J (2008) Macromolecules 41:3243–3249
35. Riess G (2003) Prog Polym Sci 28:1107–1170
36. Jenkins AD, Jones RG, Moad G (2010) Pure Appl Chem 82:483–491
37. Moad G, Rizzardo E, Thang SH (2008) Acc Chem Res 41:1133–1142
38. Matyjaszewski K, Müller AHE (eds) (2009) Controlled and living polymerizations. From mechanisms to applications. Wiley-VCH, Weinheim
39. Barner-Kowollik C (ed) (2008) Handbook of RAFT polymerization. Wiley-VCH, Weinheim
40. Moad G, Rizzardo E, Thang SH (2012) Aust J Chem 65:985–1076
41. Miasnikova A, Laschewsky A (2012) J Polym Sci, Part A: Polym Chem 50:3313–3323
42. Troll K, Kulkarni A, Wang W, Darko C, Bivigou-Koumba AM, Laschewsky A, Müller-Buschbaum P, Papadakis CM (2008) Colloid Polym Sci 286:1079–1092
43. Bivigou-Koumba AM, Kristen J, Laschewsky A, Müller-Buschbaum P, Papadakis CM (2009) Macromol Chem Phys 210:565–578
44. Adelsberger J, Kulkarni A, Jain A, Wang W, Bivigou-Koumba AM, Busch P, Pipich V, Holderer O, Hellweg T, Laschewsky A, Müller-Buschbaum P, Papadakis CM (2010) Macromolecules 43:2490–2501
45. Jain A, Kulkarni A, Bivigou-Koumba AM, Wang W, Busch P, Laschewsky A, Müller-Buschbaum P, Papadakis CM (2010) Macromol Symp 291/292:221–229
46. Adelsberger J, Meier-Koll A, Bivigou-Koumba AM, Busch P, Holderer O, Hellweg T, Laschewsky A, Müller-Buschbaum P, Papadakis CM (2011) Colloid Polym Sci 289:711–720
47. Adelsberger J, Metwalli E, Diethert A, Grillo I, Bivigou-Koumba AM, Laschewsky A, Müller-Buschbaum P, Papadakis CM (2012) Macromol Rapid Comm 33:254–259
48. Adelsberger J, Grillo I, Kulkarni A, Sharp M, Bivigou-Koumba AM, Laschewsky A, Müller-Buschbaum P, Papadakis CM (2013) Soft Matter 9:1685–1699
49. Brown W, Mortensen K (eds) (2000) Scattering in polymeric and colloidal systems. Gordon and Breach, Amsterdam
50. Grillo I (2008) Chapter 13: Small-angle neutron scattering and application in soft condensed matter. In: Borsali R, Pecore R (eds) Soft matter characterization, vol 1. Springer, New York
51. Ewen B, Richter D (1997) Adv Polym Sci 134:1–129
52. Richter D, Monkenbusch M, Arbe A, Colmenero J (2005) Adv Polym Sci 174:1–221
53. Päch M, Zehm D, Lange M, Dambowsky I, Weiss J, Laschewsky A (2010) J Am Chem Soc 132:8757–8765
54. Skrabania K, Miasnikova A, Bivigou-Koumba AM, Zehm D, Laschewsky A (2011) Polym Chem 2:2074–2083
55. Wang W, Troll K, Kaune G, Metwalli E, Ruderer M, Skrabania K, Laschewsky A, Roth SV, Papadakis CM, Müller-Buschbaum P (2008) Macromolecules 41:3209–3218
56. Wang W, Kaune G, Perlich J, Papadakis CM, Koumba AMB, Laschewsky A, Schlage K, Röhlsberger R, Roth SV, Cubitt R, Müller-Buschbaum P (2010) Macromolecules 43:2444–2452
57. Zhong Q, Wang W, Adelsberger J, Golosova A, Koumba AMB, Laschewsky A, Funari SS, Perlich J, Roth SV, Papadakis CM, Müller-Buschbaum P (2011) Colloid Polym Sci 289:569–581
58. Zhong Q, Metwalli E, Kaune G, Rawolle M, Bivigou-Koumba AM, Laschewsky A, Papadakis CM, Cubitt R, Müller-Buschbaum P (2012) Soft Matter 8:5241–5249
59. Zhong Q, Adelsberger J, Niedermeier M, Golosova A, Bivigou-Koumba AM, Laschewsky A, Funari SS, Papadakis CM, Müller-Buschbaum P (2013). Colloid Polym Sci 291:1439–1451
60. Zhong Q (2012) Structure and transition behavior of novel thermoresponsive polymer films. Doctoral thesis. Technische Universität München, München
61. Miasnikova A (2012) New hydrogel forming thermo-responsive block copolymers of increasing structural complexity. Doctoral thesis. Universität Potsdam, Potsdam
62. Winnik FM, Davidson AR, Hamer GK, Kitano H (1992) Macromolecules 25:1876–1880
63. Kujawa P, Segui F, Shaban S, Diab C, Okada Y, Tanaka F, Winnik FM (2006) Macromolecules 39:341–348
64. Koga T, Tanaka F, Motokawa R, Koizumi S, Winnik FM (2008) Macromolecules 41:9413–9422
65. Cho EC, Lee J, Cho K (2003) Macromolecules 36:9929–9934
66. Aseyev V, Hietala S, Laukkanen A, Nuopponen M, Confortini O, Prez FED, Tenhu H (2005) Polymer 46:7118–7131
67. Junk MJN, Li W, Schlüter AD, Wegner G, Spiess HW, Zhang A, Hinderberger D (2011) J Am Chem Soc 133:10832–10838
68. Nuopponen M, Kalliomäki K, Laukkanen A, Hietala S, Tenhu H (2008) J Polym Sci, Part A: Polym Chem 46:38–46
69. Farago B, Monkenbusch M, Richter D, Huang JS, Fetters LJ, Gast AP (1993) Phys Rev Lett 71:1015–1018
70. Kanaya T, Monkenbusch M, Watanabe H, Nagao M, Richter D (2005) J Chem Phys 122:144905–144913
71. Harms S, Rätzke K, Faupel F, Egger W, Ravello L, Laschewsky A, Wang W, Müller-Buschbaum P (2010) Macromol Rapid Comm 31:1364–1367
72. Wang W, Metwalli E, Perlich J, Troll K, Papadakis CM, Cubitt R, Müller-Buschbaum P (2009) Macromol Rapid Comm 30:114–119
73. Wang W, Metwalli E, Perlich J, Papadakis CM, Cubitt R, Müller-Buschbaum P (2009) Macromolecules 42:9041–9051
74. Zhou S, Wu C (1996) Macromolecules 29:4998–5001
75. Müller-Buschbaum P, Stamm M (1998) Macromolecules 31:3686–3692
76. Müller-Buschbaum P, Gutmann JS, Lorenz C, Schmitt T, Stamm M (1998) Macromolecules 31:9265–9272
77. Tanaka T, Hocker LO, Benedek GB (1973) J Chem Phys 59:5151–5159
78. Landau LD, Lifshitz EM (1986) Theory of elasticity, 3rd edn. Pergamon Press, Oxford

79. Li Y, Tanaka T (1990) J Chem Phys 92:1365–1371
80. Yan Q, Hoffman AS (1995) Polymer 36:887–889
81. Kaneko Y, Nakamura S, Sakai K, Aoyagi T, Kikuchi A, Sakurai Y, Okano T (1998) Macromolecules 31:6099–6105
82. Kaholek M, Lee W-K, Ahn S-J, Ma H, Caster KC, LaMattina B, Zauscher S (2004) Chem Mater 16:3688–3696
83. Yim H, Kent MS, Mendez S, Lopez GP, Satija S, Seo Y (2006) Macromolecules 39:3420–3426
84. Tamai Y, Tanaka H, Nakanishi K (1996) Macromolecules 29:6750–6760
85. Grinberg VY, Dubovik AS, Kuznetsov DV, Grinberg NV, Grosberg AY, Tanaka T (2000) Macromolecules 33:8685–8692
86. Okada Y, Tanaka F (2005) Macromolecules 38:4465–4471
87. Kojima H, Tanaka F (2010) Macromolecules 43:5103–5113
88. Tanaka F, Koga T, Kojima H, Winnik FM (2011) Chin J Polym Sci 29:13–21